

pubs.acs.org/JACS Article

# Targeted, Molecular Europium (III) Probes Enable Luminescence-Guided Surgery and 1 Photon Post-Surgical Luminescence Microscopy of Solid Tumors

Raphael Lengacher, Kirsten E. Martin, Dariusz Śmiłowicz, Helena Esseln, Piyusha Lotlikar, Alexei Grichine, Olivier Maury, and Eszter Boros\*



Cite This: J. Am. Chem. Soc. 2023, 145, 24358-24366



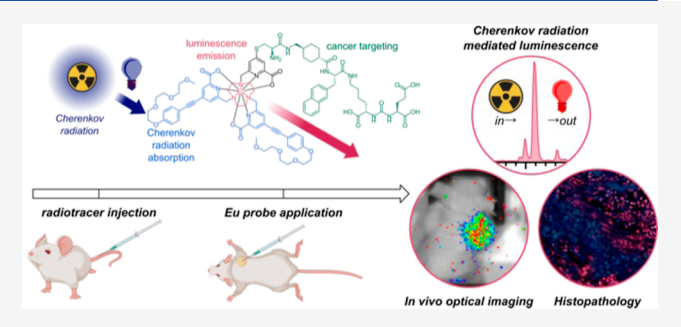
**ACCESS** I

III Metrics & More

Article Recommendations

Supporting Information

**ABSTRACT:** Discrete luminescent lanthanide complexes represent a potential alternative to organic chromophores due to their tunability of optical properties, insensitivity to photobleaching, and large pseudo-Stokes shifts. Previously, we demonstrated that the lack of depth penetration of UV excitation required to sensitize discrete terbium and europium complexes can be overcome using Cherenkov radiation emitted by clinically employed radioisotopes in situ. Here, we show that the second-generation europium complexes  $[\mathrm{Eu}^{(\mathrm{III})}(\mathrm{pcta-PEPA_2})]$  and  $[\mathrm{Eu}^{(\mathrm{III})}(\mathrm{tacn-pic-PEPA_2})]$  ( $\Phi$  = 57% and 76%, respectively) lower the limit of detection (LoD) to 1 nmol in the presence of 10  $\mu$ Ci of Cherenkov emitting isotopes,



<sup>18</sup>F and <sup>68</sup>Ga. Bifunctionalization provides access to cysteine-linked peptide conjugates with comparable brightness and LoD. The conjugate, [Eu(tacn-(pic-PSMA)-PEPA<sub>2</sub>)], displays high binding affinity to prostate-specific membrane antigen (PSMA)-expressing PC-3 prostate cancer cells in vitro and can be visualized in the membrane-bound state using confocal microscopy. Biodistribution studies with the [<sup>86</sup>Y][Y<sup>(III)</sup>(tacn-(pic-PSMA)-PEPA<sub>2</sub>)] analogue in a mouse xenograft model were employed to study pharmacokinetics. Systemic administration of the targeted Cherenkov emitter, [<sup>68</sup>Ga][Ga<sup>(III)</sup>(PSMA-617)], followed by intratumoral injection or topical application of 20 or 10 nmol [Eu<sup>(III)</sup>(tacn-(pic-PSMA)-PEPA<sub>2</sub>)], respectively, in live mice resulted in statistically significant signal enhancement using conventional small animal imaging (620 nm bandpass filter). Optical imaging informed successful tumor resection. Ex vivo imaging of the fixed tumor tissue with 1 and 2 photon excitation further reveals the accumulation of the administered Eu<sup>(III)</sup> complex in target tissues. This work represents a significant step toward the application of luminescent lanthanide complexes for optical imaging in a clinical setting.

## **■ INTRODUCTION**

The most common treatment for cancer is the surgical resection of cancerous tissue. 1-3 Accurate margin delineation is imperative; residual tumor cells can result in a resurgence of the tumor, often with lethal consequences.<sup>4,5</sup> This needs to be balanced by the preservation of as much healthy tissue as possible to keep any functional impairment to a minimum. Diagnostic tools that can better inform the surgeon's decisionmaking process are therefore desirable. Various intrasurgical imaging techniques can be employed for this purpose. Fluorescence imaging offers advantages such as high spatial and temporal resolution, a low limit of detection, and low cost while limiting the invasive nature of the procedure.<sup>8–10</sup> State of the art fluorescence-guided surgery currently relies predominantly on nontargeted constructs that are directly administered at the site of interest, 11 but "smart probes" that only accumulate in target tissues or increase/change their emissive properties in target tissues are entering preclinical and clinical trials.3,12-16

Most fluorescent probes exhibit optical properties arising from hyperconjugation of pi-/aromatic systems of organic chromophores, excitation of spin- and Laporte-allowed transitions that undergo de-excitation by vibrational de-excitation and fluorescence emission while preventing competing intersystem crossing processes. These constructs are characterized by their broad emission bands, susceptibility for photobleaching, and limited tunability of emission properties and chemical functionalization (Figure 1).

Metal-based luminescent probes can provide a potential alternative. <sup>20</sup> Specifically, lanthanide complexes have narrow

Received: August 29, 2023 Revised: October 12, 2023 Accepted: October 13, 2023 Published: October 23, 2023





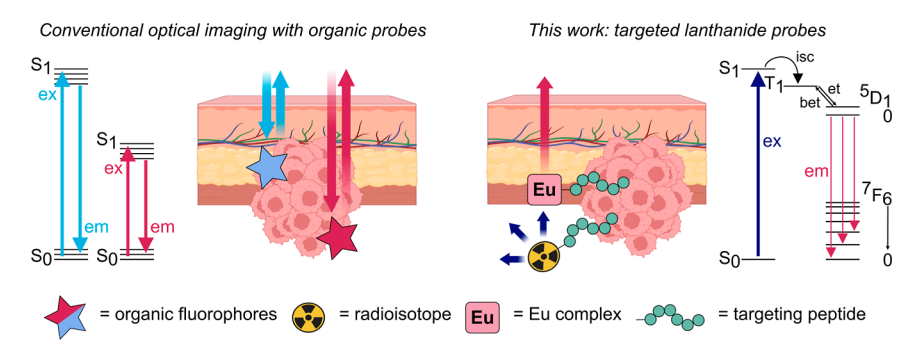


Figure 1. Comparison of optical imaging using organic fluorophores (left) with Cherenkov radiation mediated energy transfer (CRET)-based luminescent lanthanide probes (right). The corresponding Jabłoński (left) and Dieke (right) diagrams are given with ex; excitation, em; emission, isc; inter-system crossing, et; energy transfer, and bet; back energy transfer.

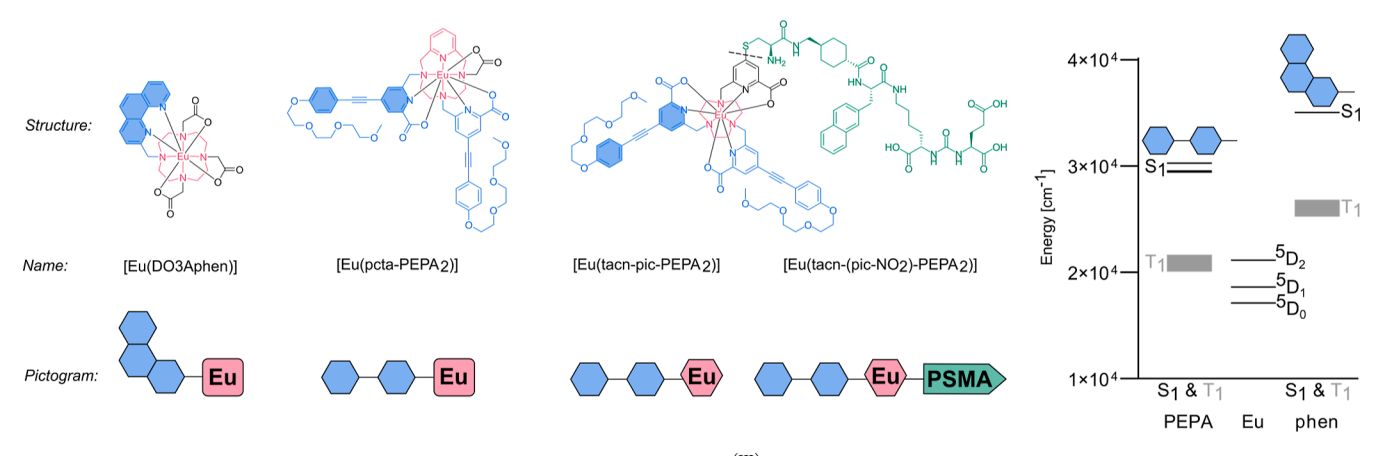


Figure 2. Lewis structures, names, and pictogram representations of the Eu(III) complexes investigated in this work. Maximum absorbance and quantum yields of the complexes are given below. A Dieke diagram comparing the singlet and estimated triplet excited states of both antennas with the emissive <sup>5</sup>D states of Eu is given on the right. Excited triplet state energies are approximated as 9000 cm<sup>-1</sup> lower than the corresponding excited singlet states, in line with literature values on similar systems.<sup>2</sup>

emission bands in the visible and near IR regions, arising from f-f orbital transitions that are characteristic of each lanthanide. 21-24 Since f-f transitions are Laporte and frequently also spin forbidden, their direct excitation is challenging. Excitation can be achieved indirectly through an organic chromophore, which populates the corresponding lanthanide excited state by energy transfer (antenna effect). 25,26 The indirect sensitization pathway renders lanthanide complexes less prone to photobleaching and degradation, while the long-lived nature of the de-excitation process provides opportunities for time-resolved imaging. Previous work by Tripiër, Maury, and Parker has demonstrated that  $Eu^{(\mathrm{III})}$  probes incorporating picolyl-aryl-alkynes can produce probes with improved quantum yields suitable for fixed cell and zebrafish imaging with  $\mathrm{Eu^{(III)}}$  and  $\mathrm{Sm^{(III)}}$  using two-photon (2P) excitation.<sup>2</sup>

A major hurdle to the in vivo application of lanthanides as optical probes is their need for either short-wave excitation <400 nm, which inherently exhibits limited tissue depth penetration, or alternatively low-intensity 2P excitation for efficient sensitization. Previously, we have demonstrated that in situ excitation by CR can provide a suitable excitation source, efficiently sensitizing Tb<sup>(III)</sup> and Eu<sup>(III)</sup> luminescence. <sup>30–32</sup> CR is emitted by radioactive isotopes that decay by emission of a charged particle with an energy greater than the threshold The clinically employed energy of 264 keV in water.3 positron-emitting radionuclides  $^{18}$ F  $(t_{1/2} = 109 \text{ min, } \beta_{\text{avg}} =$ 0.25 MeV, 97% positron decay) and <sup>68</sup>Ga ( $t_{1/2}$  = 68 min,  $\beta_{avg}$  =

0.89 MeV, 89% positron decay) are well suited for this purpose; others have also shown that radiation-induced particle emissions can be absorbed by nanoparticles and harnessed for photodynamic therapy. 34,35

Our previous work<sup>32</sup> identified Eu<sup>(III)</sup> probes as compatible with in vivo applications in small animal tumor models due to the characteristic red emission at 597 and 621 nm, which falls in the first biological window where the light absorption of tissue forms a local minimum. 36 However, the [Eu(III)(DO3Aphen)] complexes exhibited limited brightness, requiring the concurrent intratumoral administration of both the Eu(III) probe and Cherenkov emitter, indicating that significant improvements to the probe design were necessary to improve clinical viability.

Here, we demonstrate how an improved probe design and a compact functionalization approach produce the first discrete bifunctional Eu(III) complex suitable for in vitro and in vivo imaging of cancer cells. These compounds enable tumor resection via luminescence-guided surgery in a mouse xenograft model following the systemic administration of a clinical <sup>68</sup>Ga-radiopharmaceutical as the in situ excitation source. The excised, fixed tumor tissue can be subsequently analyzed for tumor margins using conventional one-photon (1P) luminescence microscopy.

## RESULTS AND DISCUSSION

Probe Design and Synthesis. Our previous chemical design incorporated a phenanthroline antenna, which did not

Table 1. Photophysical Characterization of Eu(III) Complexes in 20% EtOH in PBS at Room Temperature

complex	$\lambda_{\max}$ [nm]	$\varepsilon \ [\mathrm{M^{-1}\ cm^{-1}}]$	$\tau(H_2O)$ [ms]	$\tau(D_2O)$ [ms]	q	$\Phi$ [%]
[Eu <sup>(III)</sup> (DO3Aphen)] <sup>30</sup>	283	23,690	1.27	1.79	0	15
$[Eu^{(III)}(pcta-PEPA_2)]$	335	54,460	1.09	1.33	0	57
$[Eu^{(III)}(tacn-pic-PEPA_2)]$	336	65,230	0.87	1.13	0	76 <sup>a</sup>
$[Eu^{(III)}(tacn-(pic-NO_2)-PEPA_2]$	334	30,990	0.78	0.97	0	31
$[Eu^{(III)}(tacn-(pic-PSMA)-PEPA_2)]$	327	64,240	0.74	1.06	0	24

 $^a\Phi$  additional measurement in 100%  ${
m H_2O}$  provided in the Supporting Information, Section 1.

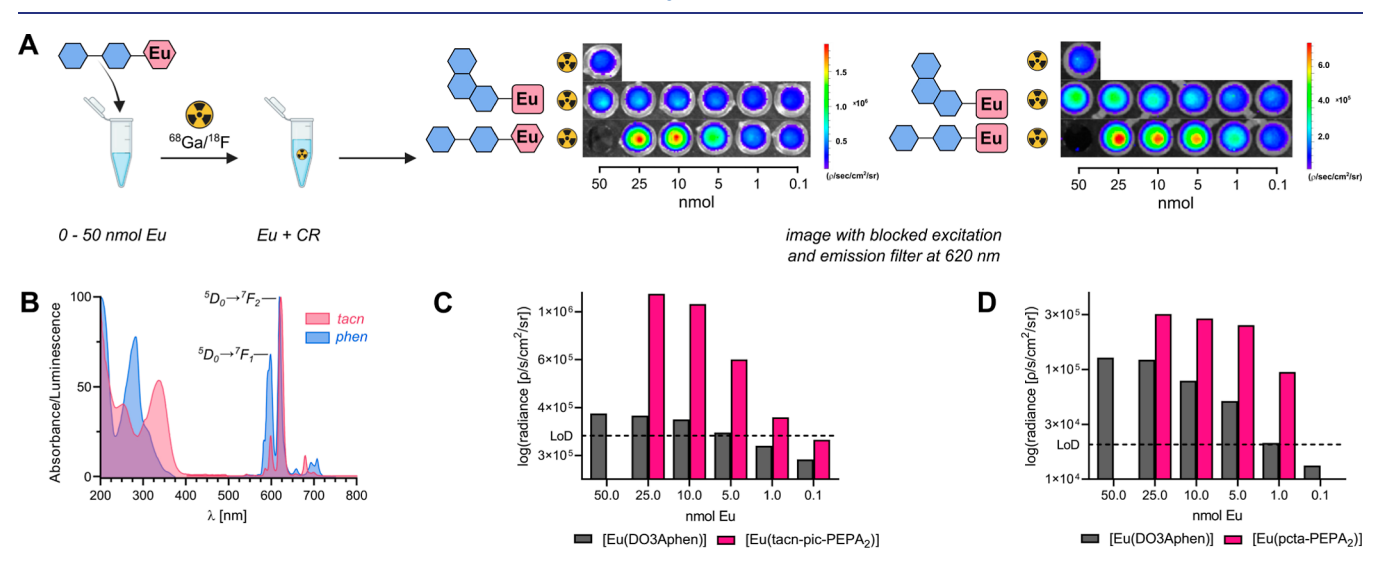


Figure 3. (A) Procedure and results of the phantom image assay of  $[Eu^{(III)}(pcta-PEPA_2)]$  and  $[Eu^{(III)}(tacn-pic-PEPA_2)]$  versus  $[Eu^{(III)}(DO3Aphen)]$  with 10  $\mu$ Ci <sup>68</sup>Ga and a <sup>68</sup>Ga only background sample. Region of interest (ROI) analysis of  $[Eu^{(III)}(tacn-pic-PEPA_2)]$  versus  $[Eu^{(III)}(DO3Aphen)]$ , shows improvement in the limit of detection (LoD) for the new probe. (B) Overlaid absorption (200–500 nm) and steady-state emission (400–800 nm) of  $[Eu^{(III)}(DO3Aphen)]$  (blue) and  $[Eu^{(III)}(tacn-pic-PEPA_2)]$  (red). (C) ROI analysis of the phantom images of  $[Eu^{(III)}(DO3Aphen)]$  and  $[Eu^{(III)}(tacn-pic-PEPA_2)]$  excited by CRET from <sup>68</sup>Ga, showing a roughly 10-fold increase in the LoD. (D) ROI analysis of the phantom images of  $[Eu^{(III)}(DO3Aphen)]$  and  $[Eu^{(III)}(pcta-PEPA_2)]$  excited by CRET from <sup>68</sup>Ga, showing a roughly 10-fold increase in the LoD.

provide appropriately strong sensitization and brightness to the corresponding Eu complex. Previous work suggests that the higher triplet state energy of the phen antenna leads to less sensitization efficiency. To address the shortcomings of these first-generation constructs, we drew inspiration from previous work on intraligand charge transfer (ILCT)optimized antennas incorporating extended  $\pi$ -conjugated systems of picolyl-functionalized aza-macrocycles to chelate Eu(III) 38-40 Specifically, we identified a pegylated aryl alkyne (PEPA) from previous work to sensitize Eu(III) with high efficiency while introducing improved solubility.<sup>27,41</sup> A Dieke diagram comparing the S1 and estimated T1 energy states of both antennas is given in Figure 2, demonstrating that aryl alkyne antennae are better suited to the direct excitation of the <sup>5</sup>D<sub>1/0</sub> states, whereas phen-mediated excitation experiences energy transfer and subsequent de-excitation from  $^5D_2$ , with less efficient energy transfer to the  $^5D_{1/0}$  states.  $^{31,37}$  We employed both tacn (1,4,7-triazacyclononane) and pyclen (1,4,7,10-tetraaza-2,6-pyridinophane) macrocyclic chelators to incorporate a macrocyclic backbone for appropriate in vivo stability. Accordingly, the pyclen-based [Eu(III)(pcta-PEPA<sub>2</sub>)] complex was synthesized following a previously published procedure. [Eu(III)(tacn-pic-PEPA2)] was synthesized by alkylating tacn with ethyl 6-(chloromethyl)picolinate under dry conditions, delivering compound 1 in 81% yield. This was followed by a second alkylation with two equiv of PEPAbromide (2) under the same conditions, providing compound

3 in a 50% yield. The basic hydrolysis of 3 to its corresponding carboxylic acid (4) using 1 M KOH proceeded in a quantitative yield. Subsequent complexation with  $Eu(OTf)_3$  resulted in the complex  $\left[Eu^{(III)}(\text{tacn-pic-PEPA}_2)\right]$  in a yield of 82% following reverse phase purification (Scheme S1.3).

Photophysical Characterization. Following the complex synthesis, we conducted photophysical characterization to quantify maximum absorption  $(\lambda_{max})$ , molar extinction coefficients  $(\varepsilon)$ , inner sphere hydration numbers (q), and quantum yields  $(\Phi)$  (Table 1). The quantum yields of [Eu<sup>(III)</sup>(pcta-PEPA<sub>2</sub>)] (57%) and [Eu<sup>(III)</sup>(tacn-pic-PEPA<sub>2</sub>)] (76%) represent a significant improvement over the firstgeneration [Eu<sup>(III)</sup>(DO3Aphen)] (15%) series and are in line with the literature reported values.<sup>32</sup> Of note, the relative intensity of emission bands shows enhancement of the <sup>5</sup>D<sub>0</sub>  $\rightarrow$  $^{7}\text{F}_{2}$  band with a concurrent decrease in intensity of  $^{5}\text{D}_{0} \rightarrow {}^{7}\text{F}_{1}$ when compared with  $[Eu^{(III)}(DO3Aphen)]$ , while  ${}^5D_0 \rightarrow {}^7F_4$ remains low in relative intensity in all cases. Next, we conducted phantom image experiments using in situ excitation with CR by <sup>18</sup>F and <sup>68</sup>Ga, with the latter providing increased photon flux due to greater positron energy (Figures 3 and S1.14). [Eu<sup>(III)</sup>(pcta-PEPA<sub>2</sub>)] and [Eu<sup>(III)</sup>(tacn-pic-PEPA<sub>2</sub>)] were doped with 9-12  $\mu$ Ci of <sup>18</sup>F and 10  $\mu$ Ci of <sup>68</sup>Ga, which corresponds to a typical quantity used in preclinical in vivo PET imaging. 42,43 Experiments were conducted side-by-side with the first-generation compound [Eu(III)(DO3Aphen)]. Complex amounts of between 0.1 and 50 nmol were prepared

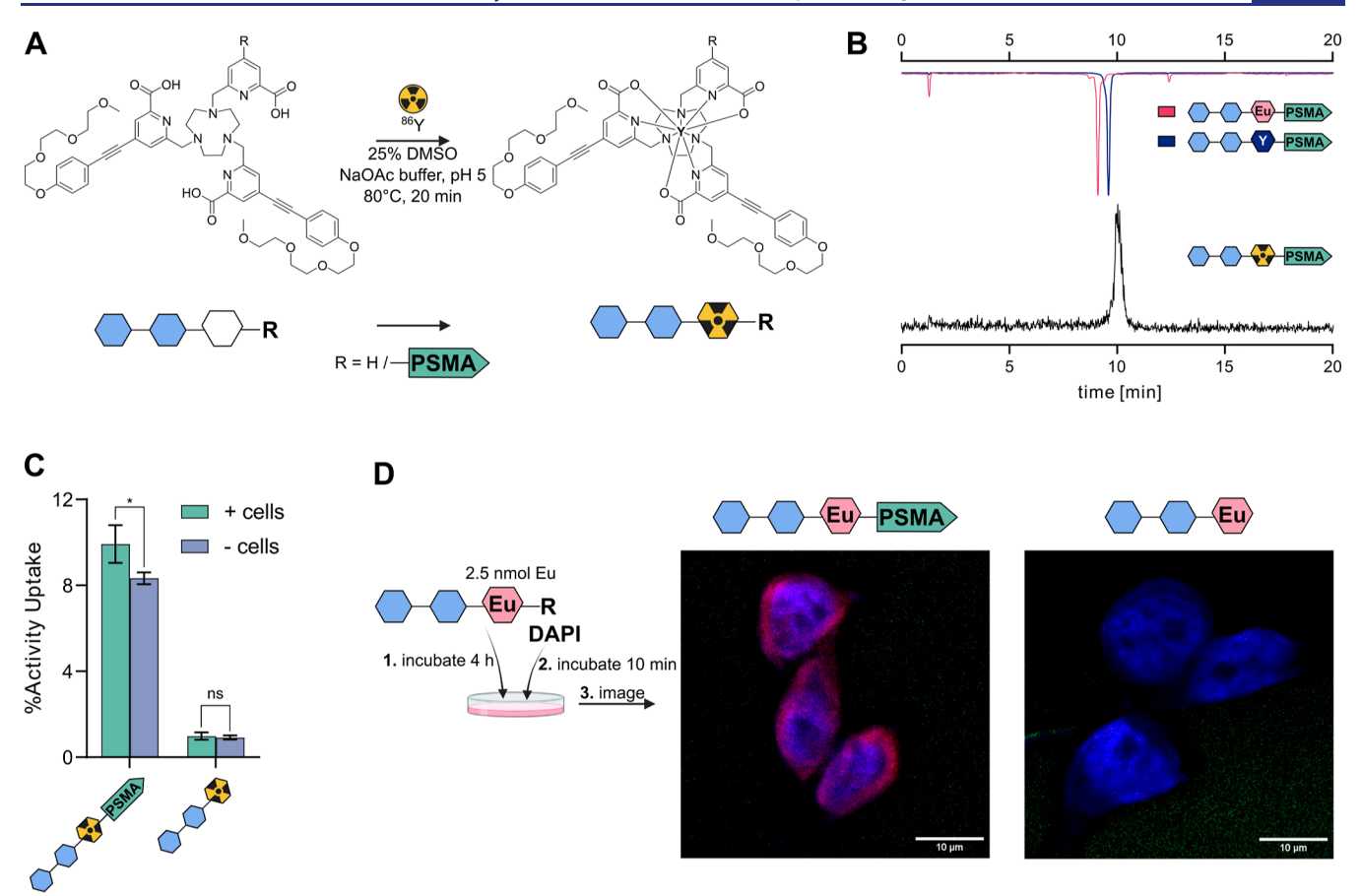


Figure 4. Scheme of the radiolabeling of tacn-pic-PEPA<sub>2</sub> and tacn-(pic-PSMA)-PEPA<sub>2</sub> with <sup>86</sup>Y and the corresponding pictograms. (B) HPLC coinjection of  $[Y^{(III)}(tacn-(pic-PSMA)-PEPA_2)]$ ,  $[Eu^{(III)}(tacn-(pic-PSMA)-PEPA_2)]$ , and  $[S^{6}Y][Y^{(III)}(tacn-(pic-PSMA)-PEPA_2)]$ . UV trace of the nonradioactive complexes inverted on top and γ trace of the radiocomplex at the bottom. (C) Results of the cell binding of  $[S^{6}Y][Y^{(III)}(tacn-(pic-PSMA)-PEPA_2)]$  and  $[S^{6}Y][Y^{(III)}(tacn-pic-PEPA_2)]$  with PSMA+ (PiP) and PSMA-(flu) PC-3 cancer cells. (D) Workflow and results for the cell staining of PSMA + PC-3 cancer cells with DAPI at different concentrations of  $[Eu^{(III)}(tacn-(pic-PSMA)-PEPA_2)]$  and  $[Eu^{(III)}(tacn-pic-PEPA_2)]$ ; red signal—Eu<sup>(III)</sup> and blue signal—DAPI.

in 20% EtOH in phosphate-buffered saline (PBS) and doped with the respective radioisotopes. Samples were imaged on a conventional small animal scanner with blocked excitation and open emission, as well as with an emission filter set to 620 nm, which prioritizes the red emission from the Eu complexes over the blue and UV CR background. Both complexes show a significant signal intensity increase of an order of magnitude compared to [Eu<sup>(III)</sup>(DO3Aphen)], which is evident from both visual inspection and quantitative assessment of the obtained images (Figure 3C,D). Based on the improved signal intensity and more straightforward synthetic accessibility, [Eu<sup>(III)</sup>(tacnpic-PEPA<sub>2</sub>)] was chosen over [Eu<sup>(III)</sup>(pcta-PEPA<sub>2</sub>)] for the synthesis of the corresponding targeted probe.

**Bioconjugation.** A significant challenge for the functionalization of aryl-alkyne picolinates is their sensitivity to acidic conditions, which limits the means to introduce peptidic targeting vectors. Therefore, we sought conjugation strategies that would enable bioconjugation at a near-terminal stage, immediately preceding or even following the complexation with the lanthanide ion. Conjugation to a cysteine thiol by way of nucleophilic aromatic substitution of the nitro-functional group of picolinate was identified as the most suitable conjugation approach. This method does not introduce additional aromatic or lipophilic elements that would further reduce compound solubility or impart photoquenching effects, as previously demonstrated by Parker for the conjugation of

Eu-phosphinate complexes<sup>28,44</sup> and, more recently, for the bioconjugation of preformed radiochemical complexes by us. 45 The corresponding [Eu<sup>(III)</sup>(tacn-(pic-NO<sub>2</sub>)-PEPA<sub>2</sub>)] complex can be obtained by stepwise alkylation of tacn, first with the pnitrobromo-picolinic acid ethyl ester (5), delivering compound 6 in a 40% yield. This was followed by alkylation with two picolyl aryl alkyne electrophiles in 52% yield. Subsequent hydrolysis with KOH provided the unprotected chelator tacn-(pic-NO<sub>2</sub>)-PEPA<sub>2</sub> (7) in 73% yield, which was then complexed with Eu(OTf)<sub>3</sub>, delivering the complex [Eu<sup>(III)</sup>(tacn-(pic-NO<sub>2</sub>)-PEPA<sub>2</sub>)] in 67% yield. This complex exhibits a reduced PEPA<sub>2</sub>)]. A targeting vector, composed of the peptide cysteine-cyclohexyl-naphtyl-KuE, a peptide sequence previously validated for the targeting of the prostate-specific membrane antigen, was reacted with [Eu(III)(tacn-(pic-NO<sub>2</sub>)-PEPA<sub>2</sub>)] in a DMF/H<sub>2</sub>O (3:1) mixture at room temperature to yield the thioconjugated species  $[Eu^{(III)}(tacn-(pic-PSMA)-PEPA_2)]$ . The quantum yield of  $[Eu^{(III)}(tacn-(pic-PSMA)-PEPA_2)]$ PEPA<sub>2</sub>)] is further reduced ( $\Phi = 24\%$ ) but still represents a significant improvement over [Eu<sup>(III)</sup>(DO3Aphen)] derivatives ( $\Phi$  < 15%). The corresponding CRET studies indicate a LoD of 1-0.1 nmol (Supporting Information, Figure S1.17 and Table 1), comparing well to the nonfunctionalized analogues.

**In Vitro Studies.** With a targeted and photophysically validated Eu<sup>(III)</sup> probe in hand, we next conducted extensive in

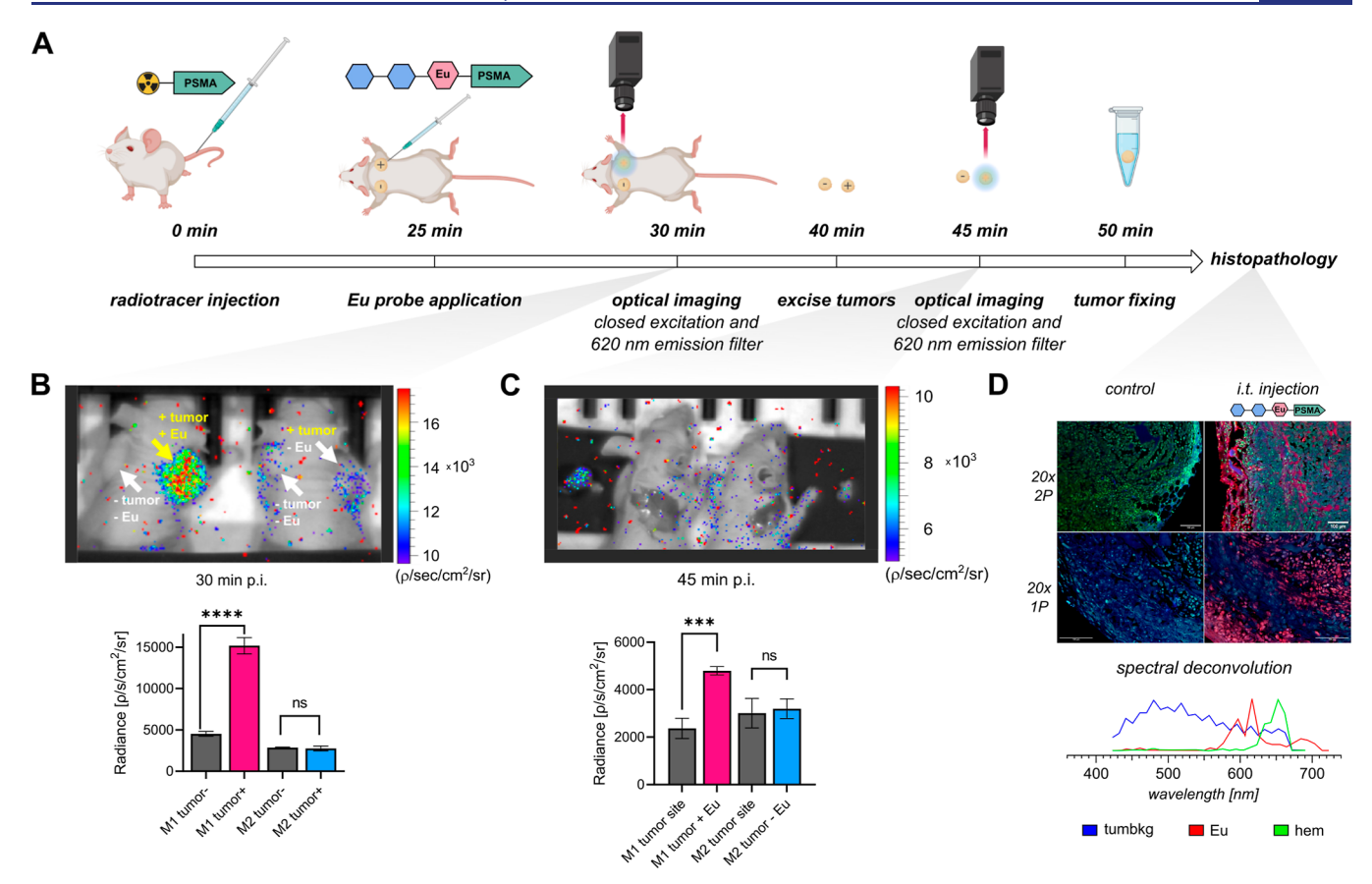


Figure 5. (A) Surgical procedure for the luminescence-guided surgery of tumor-bearing mice with [68Ga][Ga(III)(PSMA-617)] and [Eu(III)(tacn-(pic-PSMA)-PEPA<sub>2</sub>)]. (B) Presurgical optical imaging of mice bearing PSMA-positive (right shoulder) and PSMA-negative (left shoulder) tumor xenografts (data for cohort 1 is shown). Left mouse (M1) was injected with [Eu(III)(tacn-(pic-PSMA)-PEPA<sub>2</sub>)] (20 nmol) in the right tumor. Mouse on the left (M2) did not receive the Eu(III) probe. ROI analysis below shows significant signal amplification by the Eu probe. (C) Postsurgical optical imaging was performed with excised tumors. ROI analysis below shows significant signal amplification by the Eu probe. (D) Results of histopathology (blue, green = autofluorescence and red = Eu). Excitation was achieved by a 1P process with UV light and a 2P process with light at 720 nm. Control tumor shows no Eu signals. Hem emission from red blood cells was not detected in the 1P epifluorescence due to the far-red cutoff of the color camera. Spectral deconvolution below shows that the red signal is diagnostic of characteristic Eu emission bands at 597 and 621 nm. Tumbkg = tumor background autofluorescence, Eu = europium(III) emission, and hem = heme emission profile.

vitro testing. Albeit the dose of administered luminescent lanthanide should remain several orders of magnitude below doses employed for MRI contrast (0.1 mmol/kg, which would correspond to 2.5  $\mu$ mol/mouse), <sup>46</sup> establishing toxicity limits represents a relevant step toward in vivo application. To this end, we conducted cell viability assays in the presence of increasing concentrations of [Eu<sup>(III)</sup>(tacn-pic-PEPA<sub>2</sub>)] and [Eu<sup>(III)</sup>(DO3Aphen)], with the latter previously validated in vivo. No statistically significant toxicity could be observed (Figures S1.18 and S1.19).

To quantitatively measure cell binding, we took advantage of the similar ionic radius of Y<sup>(III)</sup> and Eu<sup>(III)</sup> (1.08 and 1.12 Å, respectively, for coordination number 8)<sup>47</sup> and employed the <sup>86</sup>Y isotope ( $t_{1/2} = 14.7$  h,  $\beta_{\rm avg} = 0.53$  MeV, 31% positron decay) as a Eu<sup>(III)</sup> tracer proxy—this approach has been validated previously to study the pharmacokinetics of Gd<sup>(III)</sup> (1.10 Å) contrast agents. We synthesized <sup>86</sup>Y homologues [Eu<sup>(III)</sup>(tacn-pic-PEPA<sub>2</sub>)] and [Eu<sup>(III)</sup>(tacn-(pic-PSMA)-PEPA<sub>2</sub>)] by direct radiolabeling of the corresponding chelators. The identity of the radioactive compounds was confirmed by HPLC coinjection with the corresponding <sup>nat</sup>Y isotopologues (Figures 4B and S1.20); retention times for both compounds were found to correlate well and only deviate minimally from the Eu<sup>(III)</sup> species. PC-3 prostate cancer cells

with or without the expression of the prostate-specific membrane antigen (PC-3 PiP and PC-3 flu, respectively) were incubated with the radioactive complexes [ $^{86}\mathrm{Y}$ ]-[ $\mathrm{Y}^{(\mathrm{III})}(\mathrm{tacn\text{-}pic\text{-}PEPA}_2)$ ] and [ $^{86}\mathrm{Y}$ ][ $\mathrm{Y}^{(\mathrm{III})}(\mathrm{tacn\text{-}pic\text{-}PEPA}_2)$ ]. PSMA-positive cells showed a statistically significant enhancement of bound radioactivity of 9.9%  $\pm$  0.88 when incubated with the targeted probe [ $^{86}\mathrm{Y}$ ][ $\mathrm{Y}^{(\mathrm{III})}(\mathrm{tacn\text{-}(pic\text{-}PSMA)\text{-}PEPA}_2)$ ]; however, the construct also exhibited nonspecific binding, evidenced by the activity bound to PSMA-negative PC-3 flu cells (8.33%  $\pm$  0.27). Even with a large amount of nonspecific uptake, the difference between PSMA-positive and PSMA-negative cells for the targeted probe is significant ( $p=0.04,\ n=3$ , Figure 4C). The nontargeted probe [ $^{86}\mathrm{Y}$ ][ $\mathrm{Y}^{(\mathrm{III})}(\mathrm{tacn\text{-}pic\text{-}PEPA}_2)$ ] displays little uptake in both cell lines (0.98%  $\pm$  0.17 (PiP) and 0.92%  $\pm$  0.09 (flu)).

Next, we probed the potential of [Eu<sup>(III)</sup>(tacn-pic-PEPA<sub>2</sub>)] and [Eu<sup>(III)</sup>(tacn-(pic-PSMA)-PEPA<sub>2</sub>)] to visualize the binding of target cells with fluorescence microscopy. Live PC-3 PiP cells were incubated with 0.1, 1, 2.5, or 5 nmol of either targeted or untargeted probe for 4 h at 37 °C, followed by DAPI nuclear stain at 37 °C for 10 min. Subsequently, cells were fixed with paraformaldehyde and imaged under a microscope with 2P excitation at 720 nm, followed by spectral unmixing for the DAPI and Eu<sup>(III)</sup> emissions, respectively

(Figure 4D). [Eu<sup>(III)</sup>(tacn-(pic-PSMA)-PEPA<sub>2</sub>)] shows localization in the cell membrane, in line with the localization of the transmembrane protein PSMA. Membrane-associated signal is detected with as low as 1 nmol compound/well (corresponding to a concentration of 1.4  $\mu$ M, Figure 4D), while [Eu<sup>(III)</sup>(tacn-pic-PEPA<sub>2</sub>)] does not display any accumulation in cells even with 5 nmol. Probe concentrations employed correspond well with cell staining experiments conducted with organic dyes. <sup>16</sup>

Pharmacokinetics of Systemic Administration. To approximate the pharmacokinetic behavior and tumor accumulation of [Eu(III)(tacn-(pic-PSMA)-PEPA<sub>2</sub>)], we conducted biodistribution studies and metabolite analysis with [86Y][Y(III)(tacn-(pic-PSMA)-PEPA<sub>2</sub>)]. Following radiochemical labeling with 86Y as described (vide supra), [86Y]- $[Y^{(III)}(tacn-\check{(pic-PSMA)-PEPA_2})]$  was administered by tail vein injection (n = 8) to mice bearing bilateral PC-3 tumors (PiP and flu). Probe distribution was evaluated by PET imaging at 1.5, 3.5, and 5.5 h (Figures S1.22-1.24), followed by sacrificial biodistributions at 2 and 6 h (Figures S1.25). While the probe exhibits statistically significant accumulation in the PSMA-positive tumor at the 6 h time point  $(4.8 \pm 0.01\%)$ ID/g), the overall pharmacokinetics (Figures S1.22–S1.25 and Tables S1.2–S1.3) are unfavorable for systemic administration as the probe localizes predominantly in the liver (11.7  $\pm$  0.03% ID/g at 6 h) and kidneys (28.4  $\pm$  0.03%ID/g at 6 h). Urine metabolite analysis at 2 and 6 h indicated the presence of an intact probe in vivo (Figure S1.26), motivating in vivo investigation of the corresponding Eu(III) complex. We posit that the compound's less than ideal behavior arises from the enhanced lipophilicity introduced by the antennae.

**CRET Imaging and Intrasurgical Resection of Tumor** Tissue. The less favorable pharmacokinetic behavior of [86Y][Y<sup>(III)</sup>(tacn-(pic-PSMA)-PEPA<sub>2</sub>)] following systemic administration indicated that the corresponding [Eu(III)(tacn-(pic-PSMA)-PEPA<sub>2</sub>)] complex was better suited for local administration, acting as a "scintillator" in combination with the systemically administered PET radiopharmaceutical as the in situ Cherenkov luminescence source. To determine the ideal dosage and time frame of the distribution of the PET radiopharmaceutical, [68Ga][Ga(III)(PSMA-617)]49 was administered at 4 different doses to mice bearing bilateral PC-3 xenografts. Doses ranged from 19 to 166 µCi, and animals were imaged at 60, 90, and 120 min postinjection on a small animal optical scanner (Figure S1.27), and ROI analysis was conducted with and without decay correction to determine the ideal timing for the administration of [Eu(III)(tacn-(pic-PSMA)-PEPA<sub>2</sub>)] (Figure S1.28), balancing pharmacokinetics and isotope decay. Based on this analysis, we selected administration >100  $\mu$ Ci of [68Ga][Ga<sup>(III)</sup>(PSMA-617)] and identified the time window of 15-45 min post injection as ideal to administer the Eu<sup>(III)</sup>-probe locally.

Eu<sup>(III)</sup> enhanced optical imaging was carried out using two methods of local administration to mimic possible clinical applications: [Eu<sup>(III)</sup>(tacn-(pic-PSMA)-PEPA<sub>2</sub>)] was administered via intratumoral injection or topical application to the target tumor site and allowed to interact with the PET probe via intermolecular CRET (Figure 5A). First, mice bearing bilateral xenografts with or without PSMA expression were injected with 150  $\mu$ Ci of [ $^{68}$ Ga][Ga<sup>(III)</sup> (PSMA-617)] systemically via tail vein, followed by intratumoral administration of 20 nmol of [Eu<sup>(III)</sup>(tacn-(pic-PSMA)-PEPA<sub>2</sub>)] 25 min later (cohort 1). Optical imaging was conducted using

blocked excitation and emission detection using the 620 nm bandpass filter. Figure 5 shows side-by-side experiments of animals that were administered [Eu<sup>(III)</sup>(tacn-(pic-PSMA)-PEPA<sub>2</sub>)] (left) next to animals that had received only the radiopharmaceutical (right). Statistically significant signal enhancement was detected from the tumor with colocalization with radiotracer and [Eu<sup>(III)</sup>(tacn-(pic-PSMA)-PEPA<sub>2</sub>)] when compared to that of the control animal, which showed no signal enhancement (Figure 5B). Tumors were subsequently excised and reimaged at 45 min post injection adjacent to the open surgical site in the animal; at this time point, signal enhancement was still detectable in the excised, Eu-dosed tissue, whereas no signal above background was detected from the control tumor (Figure 5C).

We also evaluated the potential of [Eu(III)(tacn-(pic-PSMA)-PEPA<sub>2</sub>)] to provide signal enhancement in the target tissue via topical application. In accordance with the previous imaging paradigm, we injected 174  $\mu$ Ci of [ $^{68}$ Ga][Ga $^{(III)}$ (PSMA-617)] systemically. The surgical site was opened, and a solution of [Eu<sup>(III)</sup>(tacn-(pic-PSMA)-PEPA<sub>2</sub>)] (10 nmol) was applied to the tumor site 25 min p.i. and subjected to optical imaging (Figure S1.31). Quantitation of the obtained imaging data indicates that topical administration of the probe is also suitable to efficiently guide surgical resection of the cancerous tissue as evidenced by postsurgical resection imaging and quantitation via ROI analysis (Supporting Information, Figure \$1.32). It is important to note that although our phantom imaging studies employed a moderate amount of radioactivity (10  $\mu$ Ci), the actual amount of [<sup>68</sup>Ga][Ga(PSMA-617)] present in the tumor following systemic administration is an order of magnitude lower ( $\sim 1 \mu Ci$ ). This further evidence shows that improvement of emission properties was crucial to achieving statistically significant and detectable emission from [Eu<sup>(III)</sup>(tacn-(pic-PSMA)-PEPA<sub>2</sub>)].

Luminescence Microscopy of Excised Tumor Tissues. Excised tumor samples were fixed with paraformaldehyde; following tissue preparation, red luminescence of samples visible by the eye was observed under UV light (Figures S1.29D,E and S1.31D,E), evidencing that [Eu(HI)(tacn-(pic-PSMA)-PEPA<sub>2</sub>)] remains intact. Subsequently, sectioned tissue samples were imaged with wide-field epifluorescence microscopy (excitation at 365 nm and emission filter at 620 nm). Samples from tissues that had received topical or intratumoral treatment of [Eu<sup>(III)</sup>(tacn-(pic-PSMA)-PEPA<sub>2</sub>)] (Figures 5D and S1.47-1.49) show clearly discernible Eu<sup>(III)</sup>based signal emission. Topical application results in Eu(III) signals arising from the sample surface with little penetration of the probe into deeper sample regions. Intratumoral injection resulted in Eu signal localizing also to deep sample regions. Samples obtained from control animals, which did not receive any Eu(III) probe, show no red emission characteristic of Euaccumulation. Confocal microscopy with 720 nm 2P excitation and spectral unmixing further confirms that the red-emission arises from Eu(III) and not from autofluorescence or other longwave emitting tissue endogenous cofactors such as hemoglobin (Figures 5D and S1.41-1.45).

# CONCLUSIONS

In conclusion, we demonstrate for the first time that discrete, bifunctional, targeted Eu<sup>(III)</sup> probes can be employed for cellular staining in culture, guided intrasurgical resection of cancerous tissue in mice, and subsequent histopathology.

We prepared the targeted probe [Eu(III)(tacn-(pic-PSMA)-PEPA<sub>2</sub>)], which exhibits a quantum yield of 24%. Phantom imaging studies evidence that 10  $\mu$ Ci of <sup>68</sup>Ga can enhance as little as 1 nmol of Eu complex, indicating that imaging at concentration levels equivalent to organic chromophores is feasible. [Eu<sup>(III)</sup>(tacn-(pic-PSMA)-PEPA<sub>2</sub>)] retains the ability to bind to PSMA as evidenced by cell imaging experiments and quantitation of uptake using the 86Y(III)-congener. Following our analysis of pharmacokinetic properties, we applied [Eu(III)(tacn-(pic-PSMA)-PEPA<sub>2</sub>)] intrasurgically in combination with the systemically administered, clinically employed PET tracer [68Ga][Ga(III)(PSMA-617)]. In situ excitation of Eu<sup>(III)</sup> emission by CRET produced by the <sup>68</sup>Ga results in 5fold optical signal amplification and enables the resection of tumor tissue. Subsequently, the robust optical properties of [Eu(III)(tacn-(pic-PSMA)-PEPA<sub>2</sub>)] enable direct histopathological analysis of excised tumor tissues using 1P and 2P luminescence microscopy without the need for further staining with fluorescent markers.

This work represents a significant evolution from our first proof-of-concept systems, which exhibited limited brightness and in vivo compatibility, posing limited clinical relevance. The combination of the second-generation Eu(III) probe with a systemically administered, clinically validated <sup>68</sup>Ga PET radiopharmaceutical as an in situ excitation source is especially attractive for prospective clinical translation. Work to improve pharmacokinetic properties while retaining the brightness of next-generation Eu(III) probes is ongoing.

# ASSOCIATED CONTENT

# Supporting Information

The Supporting Information is available free of charge at https://pubs.acs.org/doi/10.1021/jacs.3c09444.

> Experimental procedures, NMR, HRMS, and HPLC results and characterization of complexes and radiolabeling data and imaging results (PDF)

# AUTHOR INFORMATION

## **Corresponding Author**

Eszter Boros – Department of Chemistry, Stony Brook University, Stony Brook, New York 11794, United States; Department of Chemistry, University of Wisconsin-Madison, Madison, Wisconsin 53706, United States; o orcid.org/ 0000-0002-4186-6586; Email: eboros@wisc.edu

# **Authors**

Raphael Lengacher - Department of Chemistry, Stony Brook University, Stony Brook, New York 11794, United States; Department of Chemistry, University of Wisconsin-Madison, Madison, Wisconsin 53706, United States

Kirsten E. Martin – Department of Chemistry, Stony Brook University, Stony Brook, New York 11794, United States

Dariusz Śmiłowicz - Department of Chemistry, Stony Brook University, Stony Brook, New York 11794, United States; Department of Chemistry, University of Wisconsin-Madison, Madison, Wisconsin 53706, United States

Helena Esseln - Department of Chemistry, Stony Brook University, Stony Brook, New York 11794, United States Piyusha Lotlikar - Department of Chemistry, Stony Brook University, Stony Brook, New York 11794, United States

Alexei Grichine – Institute for Advanced Biosciences, Université Grenoble Alpes, Inserm U1209, CNRS, UMR 5309, 38700 La Tronche, France

Olivier Maury – Université Lyon, ENS de Lyon, CNRS, Laboratoire de Chimie UMR 5182, F-69342 Lyon, France; orcid.org/0000-0002-4639-643X

Complete contact information is available at: https://pubs.acs.org/10.1021/jacs.3c09444

#### **Author Contributions**

All authors have given their approval to the final version of the manuscript.

#### Funding

This research was supported by the SNSF P500PN 214,250, NIBIB R21EB030071-01A1, and NSF CAREER 1942434 grants.

#### **Notes**

The authors declare no competing financial interest.

## **ACKNOWLEDGMENTS**

We would like to acknowledge the technical support provided by the Research Histology Core Laboratory, Department of Pathology, Stony Brook Medicine; Prof. Scott Laughlin and Prof. Raphaël Tripiër are acknowledged for helpful discussions pertaining to conducting confocal microscopy of fixed cells and tissue samples.

#### ABBREVIATIONS

1P, one photon; 2P, two photon; bet, back energy transfer; CR, Cherenkov radiation; CRET, Cherenkov radiation mediated energy transfer; DAPI, 2-(4-amidinophenyl)-1Hindole-6-carboxamide; em, emission; et, energy transfer; ex, excitation; ILCT, intraligand charge transfer; isc, intersystem crossing; LoD, limit of detection; p.i., post injection; PET, positron emission tomography; pyclen, 1,4,7,10-tetraaza-2,6pyridinophane; ROI, region of interest; tacn, 1,4,7-triazacyclononane

## REFERENCES

- (1) Siegel, R.; DeSantis, C.; Virgo, K.; Stein, K.; Mariotto, A.; Smith, T.; Cooper, D.; Gansler, T.; Lerro, C.; Fedewa, S.; Lin, C.; Leach, C.; Cannady, R. S.; Cho, H.; Scoppa, S.; Hachey, M.; Kirch, R.; Jemal, A.; Ward, E. Cancer treatment and survivorship statistics, 2012. Ca-Cancer J. Clin. 2012, 62 (4), 220-241.
- (2) DeSantis, C. E.; Lin, C. C.; Mariotto, A. B.; Siegel, R. L.; Stein, K. D.; Kramer, J. L.; Alteri, R.; Robbins, A. S.; Jemal, A. Cancer treatment and survivorship statistics, 2014. Ca-Cancer J. Clin. 2014, 64 (4), 252-271.
- (3) Ofori, L. O.; Withana, N. P.; Prestwood, T. R.; Verdoes, M.; Brady, J. J.; Winslow, M. M.; Sorger, J.; Bogyo, M. Design of Protease Activated Optical Contrast Agents That Exploit a Latent Lysosomotropic Effect for Use in Fluorescence-Guided Surgery. ACS Chem. Biol. 2015, 10 (9), 1977-1988.
- (4) Hiroshima, Y.; Maawy, A.; Zhang, Y.; Murakami, T.; Momiyama, M.; Mori, R.; Matsuyama, R.; Chishima, T.; Tanaka, K.; Ichikawa, Y.; Endo, I.; Hoffman, R. M.; Bouvet, M. Fluorescence-guided surgery, but not bright-light surgery, prevents local recurrence in a pancreatic cancer patient derived orthotopic xenograft (PDOX) model resistant to neoadjuvant chemotherapy (NAC). Pancreatology 2015, 15 (3),
- (5) Kato, K.; Yamada, S.; Sugimoto, H.; Kanazumi, N.; Nomoto, S.; Takeda, S.; Kodera, Y.; Morita, S.; Nakao, A. Prognostic Factors for Survival After Extended Pancreatectomy for Pancreatic Head Cancer:

- Influence of Resection Margin Status on Survival. *Pancreas* **2009**, 38 (6), 605–612.
- (6) Lauwerends, L. J.; van Driel, P. B. A. A.; Baatenburg de Jong, R. J.; Hardillo, J. A. U.; Koljenovic, S.; Puppels, G.; Mezzanotte, L.; Löwik, C. W. G. M.; Rosenthal, E. L.; Vahrmeijer, A. L.; Keereweer, S. Real-time fluorescence imaging in intraoperative decision making for cancer surgery. *Lancet Oncol.* **2021**, 22 (5), e186–e195.
- (7) Bai, M.; J Bornhop, D. Recent advances in receptor-targeted fluorescent probes for in vivo cancer imaging. *Curr. Med. Chem.* **2012**, 19 (28), 4742–4758.
- (8) Wang, X.; Li, P.; Zhang, W.; Tang, B. Recent advances in fluorescence imaging of bioactive molecules in neurons and in vivo. *Chin. J. Anal. Chem.* **2019**, 47 (10), 1537–1548.
- (9) Rudin, M.; Weissleder, R. Molecular imaging in drug discovery and development. *Nat. Rev. Drug Discovery* **2003**, *2* (2), 123–131.
- (10) Bednar, B.; Zhang, G.-J.; Williams, D. L., Jr.; Hargreaves, R.; Sur, C. Optical molecular imaging in drug discovery and clinical development. *Expert Opin. Drug Discov.* **2007**, 2 (1), 65–85.
- (11) Galema, H. A.; Meijer, R. P.; Lauwerends, L. J.; Verhoef, C.; Burggraaf, J.; Vahrmeijer, A. L.; Hutteman, M.; Keereweer, S.; Hilling, D. E. Fluorescence-guided surgery in colorectal cancer; A review on clinical results and future perspectives. *Eur. J. Surg. Oncol.* **2022**, 48 (4), 810–821.
- (12) Haque, A.; Faizi, M. S. H.; Rather, J. A.; Khan, M. S. Next generation NIR fluorophores for tumor imaging and fluorescence-guided surgery: A review. *Bioorg. Med. Chem.* **2017**, 25 (7), 2017–2034.
- (13) Low, P. S.; Singhal, S.; Srinivasarao, M. Fluorescence-guided surgery of cancer: applications, tools and perspectives. *Curr. Opin. Chem. Biol.* **2018**, *45*, 64–72.
- (14) Leopoldo, M.; Lacivita, E.; Berardi, F.; Perrone, R. Developments in fluorescent probes for receptor research. *Drug Discovery Today* **2009**, *14* (13–14), 706–712.
- (15) Slooter, M. D.; Handgraaf, H. J. M.; Boonstra, M. C.; van der Velden, L.-A.; Bhairosingh, S. S.; Que, I.; de Haan, L. M.; Keereweer, S.; van Driel, P. B. A. A.; Chan, A.; Kobayashi, H.; Vahrmeijer, A. L.; Löwik, C. W. Detecting tumour-positive resection margins after oral cancer surgery by spraying a fluorescent tracer activated by gamma-glutamyltranspeptidase. *Oral Oncol.* **2018**, *78*, 1–7.
- (16) Baranski, A.-C.; Schäfer, M.; Bauder-Wüst, U.; Roscher, M.; Schmidt, J.; Stenau, E.; Simpfendörfer, T.; Teber, D.; Maier-Hein, L.; Hadaschik, B.; et al. PSMA-11-derived dual-labeled PSMA Inhibitors for preoperative PET imaging and precise fluorescence-guided surgery of prostate cancer. *J. Nucl. Med.* **2018**, *59* (4), *639*–*645*.
- (17) Kovar, J. L.; Simpson, M. A.; Schutz-Geschwender, A.; Olive, D. M. A systematic approach to the development of fluorescent contrast agents for optical imaging of mouse cancer models. *Anal. Biochem.* **2007**, 367 (1), 1–2.
- (18) Grimm, J. B.; Lavis, L. D. Caveat fluorophore: an insiders' guide to small-molecule fluorescent labels. *Nat. Methods* **2022**, *19* (2), 149–158.
- (19) Yang, X.; Zhanghao, K.; Wang, H.; Liu, Y.; Wang, F.; Zhang, X.; Shi, K.; Gao, J.; Jin, D.; Xi, P. Versatile Application of Fluorescent Quantum Dot Labels in Super-resolution Fluorescence Microscopy. *ACS Photonics* **2016**, *3* (9), 1611–1618.
- (20) Parker, D.; Fradgley, J. D.; Wong, K.-L. The design of responsive luminescent lanthanide probes and sensors. *Chem. Soc. Rev.* **2021**, *50* (14), 8193–8213.
- (21) Wang, R.; Zhang, F. CHAPTER 1 Lanthanide-Based Near Infrared Nanomaterials for Bioimaging. In *Near-infrared Nanomaterials: Preparation, Bioimaging and Therapy Applications*; The Royal Society of Chemistry, 2016, pp 1–39.
- (22) Werts, M. H. V. Making sense of Lanthanide Luminescence. *Sci. Prog.* **2005**, 88 (2), 101–131.
- (23) Bünzli, J.-C. G. On the design of highly luminescent lanthanide complexes. *Coord. Chem. Rev.* **2015**, 293–294, 19–47.
- (24) Mathieu, E.; Sipos, A.; Demeyere, E.; Phipps, D.; Sakaveli, D.; Borbas, K. E. Lanthanide-based tools for the investigation of cellular environments. *Chem. Commun.* **2018**, *54* (72), 10021–10035.

- (25) Heffern, M. C.; Matosziuk, L. M.; Meade, T. J. Lanthanide Probes for Bioresponsive Imaging. *Chem. Rev.* **2014**, *114* (8), 4496–4539
- (26) Moore, E. G.; Samuel, A. P. S.; Raymond, K. N. From Antenna to Assay: Lessons Learned in Lanthanide Luminescence. *Acc. Chem. Res.* **2009**, 42 (4), 542–552.
- (27) Hamon, N.; Roux, A.; Beyler, M.; Mulatier, J.-C.; Andraud, C.; Nguyen, C.; Maynadier, M.; Bettache, N.; Duperray, A.; Grichine, A.; Brasselet, S.; Gary-Bobo, M.; Maury, O.; Tripier, R. Pyclen-Based Ln(III) Complexes as Highly Luminescent Bioprobes for In Vitro and In Vivo One- and Two-Photon Bioimaging Applications. *J. Am. Chem. Soc.* 2020, 142 (22), 10184–10197.
- (28) Starck, M.; Fradgley, J. D.; Di Vita, S.; Mosely, J. A.; Pal, R.; Parker, D. Targeted Luminescent Europium Peptide Conjugates: Comparative Analysis Using Maleimide and para-Nitropyridyl Linkages for Organelle Staining. *Bioconjugate Chem.* **2020**, 31 (2), 229–240.
- (29) Butler, S. J.; Lamarque, L.; Pal, R.; Parker, D. EuroTracker dyes: highly emissive europium complexes as alternative organelle stains for live cell imaging. *Chem. Sci.* **2014**, *5* (5), 1750–1756.
- (30) Cosby, A. G.; Ahn, S. H.; Boros, E. Cherenkov Radiation-Mediated In Situ Excitation of Discrete Luminescent Lanthanide Complexes. *Angew. Chem., Int. Ed.* **2018**, *57* (47), 15496–15499.
- (31) Cosby, A. G.; Woods, J. J.; Nawrocki, P.; Sørensen, T. J.; Wilson, J. J.; Boros, E. Accessing lanthanide-based, in situ illuminated optical turn-on probes by modulation of the antenna triplet state energy. *Chem. Sci.* **2021**, *12* (27), 9442–9451.
- (32) Martin, K. E.; Cosby, A. G.; Boros, E. Multiplex and In Vivo Optical Imaging of Discrete Luminescent Lanthanide Complexes Enabled by In Situ Cherenkov Radiation Mediated Energy Transfer. *J. Am. Chem. Soc.* **2021**, 143 (24), 9206–9214.
- (33) Shaffer, T. M.; Pratt, E. C.; Grimm, J. Utilizing the power of Cerenkov light with nanotechnology. *Nat. Nanotechnol.* **2017**, *12* (2), 106–117.
- (34) Zhang, Y.; Hao, Y.; Chen, S.; Xu, M. Photodynamic Therapy of Cancers With Internal Light Sources: Chemiluminescence, Bioluminescence, and Cerenkov Radiation. *Front. Chem.* **2020**, *8*, 561976.
- (35) Lengacher, R.; Marlin, A.; Smiłowicz, D.; Boros, E. Medicinal inorganic chemistry challenges, opportunities and guidelines to develop the next generation of radioactive, photoactivated and active site inhibiting metal-based medicines. *Chem. Soc. Rev.* **2022**, *51* (18), 7715–7731.
- (36) Hemmer, E.; Benayas, A.; Légaré, F.; Vetrone, F. Exploiting the biological windows: current perspectives on fluorescent bioprobes emitting above 1000 nm. *Nanoscale Horiz.* **2016**, *1* (3), 168–184.
- (37) Latva, M.; Takalo, H.; Mukkala, V.-M.; Matachescu, C.; Rodríguez-Ubis, J. C.; Kankare, J. Correlation between the lowest triplet state energy level of the ligand and lanthanide(III) luminescence quantum yield. *J. Lumin.* 1997, 75 (2), 149–169.
- (38) Walton, J. W.; Bourdolle, A.; Butler, S. J.; Soulie, M.; Delbianco, M.; McMahon, B. K.; Pal, R.; Puschmann, H.; Zwier, J. M.; Lamarque, L.; Maury, O.; Andraud, C.; Parker, D. Very bright europium complexes that stain cellular mitochondria. *Chem. Commun.* **2013**, 49 (16), 1600–1602.
- (39) Soulié, M.; Latzko, F.; Bourrier, E.; Placide, V.; Butler, S. J.; Pal, R.; Walton, J. W.; Baldeck, P. L.; Le Guennic, B.; Andraud, C.; et al. Comparative Analysis of Conjugated Alkynyl Chromophore-Triazacyclononane Ligands for Sensitized Emission of Europium and Terbium. *Chem.—Eur. J.* **2014**, 20 (28), 8636–8646.
- (40) Bui, A. T.; Roux, A.; Grichine, A.; Duperray, A.; Andraud, C.; Maury, O. Twisted Charge-Transfer Antennae for Ultra-Bright Terbium (III) and Dysprosium (III) Bioprobes. *Chem.—Eur. J.* **2018**, 24 (14), 3408–3412.
- (41) Hamon, N.; Galland, M.; Le Fur, M.; Roux, A.; Duperray, A.; Grichine, A.; Andraud, C.; Le Guennic, B.; Beyler, M.; Maury, O.; et al. Combining a pyclen framework with conjugated antenna for the design of europium and samarium luminescent bioprobes. *Chem. Commun.* **2018**, *54* (48), 6173–6176.

- (42) Meimetis, L. G.; Boros, E.; Carlson, J. C.; Ran, C.; Caravan, P.; Weissleder, R. Bioorthogonal Fluorophore Linked DFO— Technology Enabling Facile Chelator Quantification and Multimodal Imaging of Antibodies. *Bioconjugate Chem.* **2016**, 27 (1), 257–263.
- (43) Adams, C. J.; Wilson, J. J.; Boros, E. Multifunctional desferrichrome analogues as versatile 89Zr (IV) chelators for immunoPET probe development. *Mol. Pharmaceutics* **2017**, *14* (8), 2831–2842.
- (44) Shah, A.; Roux, A.; Starck, M.; Mosely, J. A.; Stevens, M.; Norman, D. G.; Hunter, R. I.; El Mkami, H.; Smith, G. M.; Parker, D.; Lovett, J. E. A Gadolinium Spin Label with Both a Narrow Central Transition and Short Tether for Use in Double Electron Electron Resonance Distance Measurements. *Inorg. Chem.* **2019**, *58* (5), 3015–3025.
- (45) Lengacher, R.; Cosby, A. G.; Śmiłowicz, D.; Boros, E. Validation of a post-radiolabeling bioconjugation strategy for radioactive rare earth complexes with minimal structural footprint. *Chem. Commun.* **2022**, *58* (99), 13728–13730.
- (46) Mikawa, M.; Kato, H.; Okumura, M.; Narazaki, M.; Kanazawa, Y.; Miwa, N.; Shinohara, H. Paramagnetic Water-Soluble Metallofullerenes Having the Highest Relaxivity for MRI Contrast Agents. *Bioconjugate Chem.* **2001**, *12* (4), 510–514.
- (47) Shannon, R. D. Revised effective ionic radii and systematic studies of interatomic distances in halides and chalcogenides. *Acta Crystallogr., Sect. A: Cryst. Phys., Diffr., Theor. Gen. Crystallogr.* **1976**, 32, 751–767.
- (48) Le Fur, M.; Rotile, N. J.; Correcher, C.; Clavijo Jordan, V.; Ross, A. W.; Catana, C.; Caravan, P. Yttrium-86 Is a Positron Emitting Surrogate of Gadolinium for Noninvasive Quantification of Whole-Body Distribution of Gadolinium-Based Contrast Agents. *Angew. Chem., Int. Ed.* **2020**, 59 (4), 1474–1478.
- (49) Afshar-Oromieh, A.; Hetzheim, H.; Kratochwil, C.; Benesova, M.; Eder, M.; Neels, O. C.; Eisenhut, M.; Kübler, W.; Holland-Letz, T.; Giesel, F. L.; et al. The theranostic PSMA ligand PSMA-617 in the diagnosis of prostate cancer by PET/CT: biodistribution in humans, radiation dosimetry, and first evaluation of tumor lesions. *J. Nucl. Med.* **2015**, *56* (11), 1697–1705.